

Communication

4-(Tris(4-methyl-1*H*-pyrazol-1-yl)methyl)aniline

Bradley B. Garrison ^{1,†}, Joseph E. Duhamel ^{1,†} , Nehemiah Antoine ^{1,†}, Steven J. K. Symes ¹ , Kyle A. Grice ² , Colin D. McMillen ^{3,*}  and Jared A. Pienkos ^{1,*}

¹ Department of Chemistry and Physics, The University of Tennessee at Chattanooga, Chattanooga, TN 37403, USA; baker-garrison@mocs.utc.edu (B.B.G.); joseph-duhamel@mocs.utc.edu (J.E.D.); nhh872@mocs.utc.edu (N.A.); steven-symes@utc.edu (S.J.K.S.)

² Department of Chemistry and Biochemistry, DePaul University, 1110 West Belden Ave, McGowan South Suite 100, Chicago, IL 60614, USA; kgrice1@depaul.edu

³ Department of Chemistry, Clemson University, Clemson, SC 29634, USA

* Correspondence: cmcmill@clemson.edu (C.D.M.); jared-pienkos@utc.edu (J.A.P.)

† These authors contributed equally to this work.

Abstract: 4-(tris(4-methyl-1*H*-pyrazol-1-yl)methyl)aniline was prepared in a 63% yield utilizing a C–F activation strategy from a mixture of 4-(trifluoromethyl)aniline, 4-methylpyrazole, and KOH in dimethylsulfoxide (DMSO). The identity of the product was confirmed by nuclear magnetic resonance spectroscopy, infrared spectroscopy, mass spectrometry, and single-crystal analysis. An analysis of crystals grown from the layering method (CH₂Cl₂/acetone/pentane) indicated two distinct polymorphs of the title compound. Moreover, density functional theory calculations utilizing the MN15L density functional and the def2-TZVP basis set indicated that 4-(tris(4-methyl-1*H*-pyrazol-1-yl)methyl)aniline forms with similar energetics to the previously reported unmethylated analog.

Keywords: tris(pyrazolyl)methane; ligand; C–F activation; crystallography; polymorphs; DFT



Citation: Garrison, B.B.; Duhamel, J.E.; Antoine, N.; Symes, S.J.K.; Grice, K.A.; McMillen, C.D.; Pienkos, J.A. 4-(Tris(4-methyl-1*H*-pyrazol-1-yl)methyl)aniline. *Molbank* **2024**, *2024*, M1823. <https://doi.org/10.3390/M1823>

Academic Editor: Nicholas Leadbeater

Received: 30 March 2024

Revised: 6 May 2024

Accepted: 8 May 2024

Published: 17 May 2024



Copyright: © 2024 by the authors. Licensee MDPI, Basel, Switzerland. This article is an open access article distributed under the terms and conditions of the Creative Commons Attribution (CC BY) license (<https://creativecommons.org/licenses/by/4.0/>).

1. Introduction

Tris(pyrazolyl)methane (Tpm) ligands (Figure 1a) and their corresponding metal complexes have been exploited for a broad range of applications, including catalysis and biomedical chemistry [1–3]. For instance, the molecule [TpmMn(CO)₃]PF₆ has been investigated as a chemotherapeutic to treat colon cancer [4]. The neutral Tpm ligands are isoelectronic analogs of the anionic tris(pyrazolyl)borate (Tp) ligands [5] (Figure 1b), another class of tridentate ligands that have also been utilized in many applications [6–8]. Of note, Tp*Rh(CO)₂ (where Tp* = HB-Pz₃*, Pz* = 3,5-dimethylpyrazolyl) has been utilized to activate C–H bonds [9]. Both the Tp and Tpm ligands were reported by Trofimenko, with the preliminary study of Tp ligands demonstrating that these ligands could bind to both early and late transition metal complexes [10]. Later, Elguero et al. developed an improved synthesis of Tp ligands that exploited a phase transfer catalyst, tetrabutylammonium (TBA) bisulfate [11]. Current methods for generating Tp ligands still exploit phase transfer catalysts and have been utilized to synthesize a variety of Tp derivatives where substituents are added to the pyrazole ring, often providing desirable steric features for their corresponding metal complexes [3]. A disadvantage of this strategy is the long reaction time that is required. For example, a recent report describing the synthesis of the tris(1-pyrazolyl)methane ligand utilizing the TBABr phase transfer catalyst requires a 3-day heating period at 70 °C [12].

In some instances, only a short heating period is required to generate Tp ligands. A report by Liddle et al. describes a C–F activation strategy to synthesize Tp ligands (Figure 1c) that requires only a 1 h reflux in DMSO [13]. Our group has also exploited such a strategy to generate Tp derivatives, including a bitopic Tp ligand [14]. Inspired by Liddle’s work, we aim to utilize this C–F activation strategy to generate Tp ligands with functionalized pyrazole rings. Herein, we report the synthesis and characterization of

4-(tris(4-methyl-1*H*-pyrazol-1-yl)methyl)aniline (**1**), highlighting that the C–F activation strategy can be utilized with substituted pyrazoles.

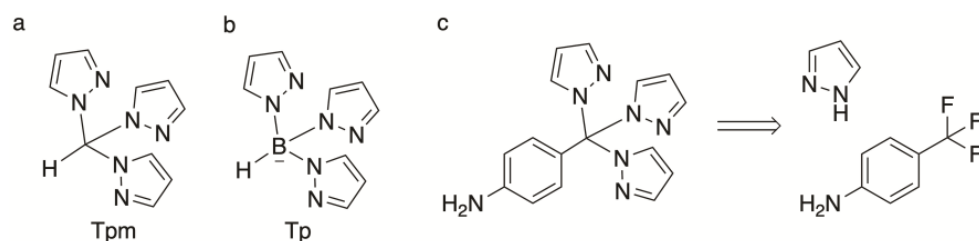
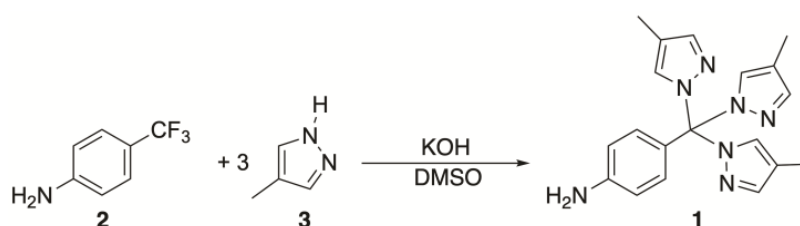


Figure 1. Tris(pyrazolyl)methane (a), tris(pyrazolyl)borate (b), and C–F activation strategy (c) exploited by Liddle et al. [13].

2. Results and Discussion

2.1. Synthesis

4-(tris(4-methyl-1*H*-pyrazol-1-yl)methyl)aniline (**1**) was prepared by refluxing a mixture of KOH, 4-(trifluoromethyl)aniline (**2**), and 4-methylpyrazole (**3**) in DMSO for 1 h (Scheme 1). Multiple aqueous washes were required to remove the DMSO from the crude product mixture. Purification by column chromatography and subsequent Et₂O washes afforded **1** as determined by multiple analytical methods: nuclear magnetic resonance (NMR), infrared (IR) spectroscopy, mass spectrometry (MS), and X-ray crystallography.



Scheme 1. Synthesis of title compound.

2.2. Characterization

¹H-NMR spectroscopy provided initial evidence for the newly synthesized Tpm derivative (**1**). The symmetry of this species provided six unique hydrogen environments. The signature features of this compound include the downfield singlets at 7.50 and 7.25 ppm corresponding to the pyrazole hydrogens, the doublets at 6.88 and 6.62 ppm corresponding to the hydrogens on the aniline ring, a broad singlet at 3.85 ppm corresponding to the N–H protons, and the upfield singlet at 2.05 ppm corresponding to the methyl groups on the pyrazole rings. ¹³C-NMR indicated nine unique chemical environments, including four quaternary carbons, which is consistent with the symmetry of this species. HSQC and HMBC data were utilized to confirm our NMR assignments (e.g., no C–H correlation was observed for the broad singlet at 3.85 ppm). Specific assignments of the ¹H and ¹³C resonances are reported in the Supplemental Information section (Figure S4).

Mass spectrometry data supported product formation with peaks at *m/z* 370.0 and 717.2 corresponding to sodium (Na⁺) adducts of our complex (respectively, [C₁₉H₂₁N₇ + Na⁺] and [(C₁₉H₂₁N₇)₂ + Na⁺]). The base peak in the mass spectrum (*m/z* 266.0) corresponded to the loss of a pyrazole ligand from the complex [M – 81]⁺ (Figure 2, compound **4**). The loss of one of the pyrazoles during electrospray is plausible considering the capillary and cone voltages and the fact that resonance from the aniline would stabilize the resulting carbocation (Figure 2).

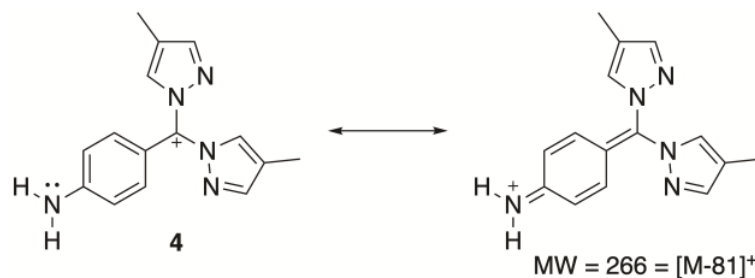


Figure 2. Structure of the compound associated with the base peak in the mass spectrum.

IR spectroscopy confirmed the presence of aromatic rings (1626 cm^{-1}) and the aniline N-H stretches (3328 cm^{-1} and 3448 cm^{-1}). These assignments were confirmed by performing DFT calculations. Optimization and frequency calculations were performed at the MN15L/def2-TZVP level on 4-(tris(4-methyl-1H-pyrazol-1-yl)methyl)aniline (**1**). The visualization of the calculated frequencies of 1628 cm^{-1} to 1639 cm^{-1} indicated they were due to the aromatic rings. The calculated frequencies of 3291 cm^{-1} and 3533 cm^{-1} corresponded to the N-H bond stretches. The calculations are consistent with the experimental IR data.

2.3. Solid-State Structure and Polymorphism

Single crystals of 4-(tris(4-methyl-1H-pyrazol-1-yl)methyl)aniline (**1**) were grown by layering a CH_2Cl_2 solution of the title compound with acetone followed by pentane. Growth in a standard NMR tube yielded two distinct morphologies—blocklike crystals (polymorph I) and tabular crystals (polymorph II). Single-crystal X-ray diffraction indeed revealed these to be two different polymorphs of the title compound (Figure 3). Polymorph I crystallizes in space group $P2_1/n$, while polymorph II crystallizes in space group $C2/c$ (Supporting Information, Table S1). The polymorphs may be considered to have a rotamer relationship with one another, where fixing the orientation of the aniline substituent leads to differing orientations of the N-N bonds and methyl groups of the methylpyrazolyl substituents (Figure 3, overlay). The mean-plane-to-mean-plane angles between the substituent rings are summarized in Table 1. In polymorph I, two of the methylpyrazolyl rings begin to approach coplanarity ($22.66(10)^\circ$), which is not the case in polymorph II, where the same methylpyrazolyl rings are more significantly inclined to one another ($57.19(11)^\circ$). In this way, polymorph II more closely resembles the structure of 4-(tri(1H-pyrazol-1-yl)methyl)aniline (CSD refcode HIXLIK), where the shallowest dihedral angle between pyrazolyl rings is 44.37° [13].

Both polymorphs feature intermolecular N-H \cdots N interactions between the NH_2 group of the aniline substituent and the N6 acceptor atom of a neighboring molecule (Table 2). The differing rotamer orientation of the nitrogen atoms in the polymorphs, however, leads to different long-range packing patterns from these interactions (Figure 4). In polymorph I, the N-H \cdots N interactions are coupled to create dimers of neighboring molecules. These dimers are then extended into a one-dimensional long-range structure via C-H \cdots N interactions, where the chains of dimers propagate along the a -axis (Supporting Information, Figure S9). In polymorph II, the N-H \cdots N interactions form the one-dimensional long-range structure without additional assistance. These chains propagate along the $[-1\ 1\ 0]$ crystallographic direction. The N-H \cdots N chain arrangement in polymorph II is again more closely aligned with what occurs in 4-(tri(1H-pyrazol-1-yl)methyl)aniline (Figure 5, compound 5), though the significant corrugation in the chains of **5** does provide a notable distinction with the straight chains of polymorph II.

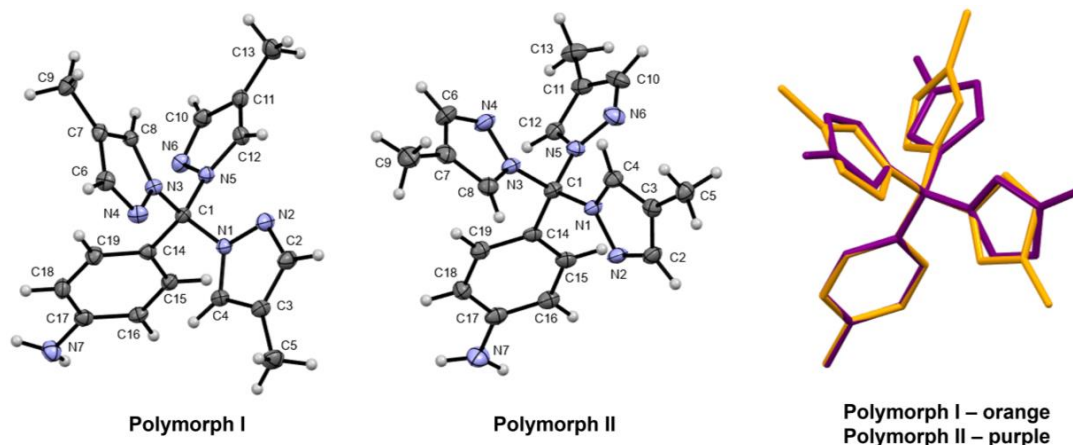


Figure 3. Crystal structure of polymorphs I and II of compound 1. The molecules are oriented similarly with respect to the central carbon atom and the aniline substituent. Ellipsoids are shown at a 50% probability level. The overlaid wireframe structures of the polymorphs (polymorph I in orange and polymorph II in purple) again keeps a consistent orientation of the central carbon atom and the aniline substituent.

Table 1. Mean-plane angles (degrees) between substituent rings in polymorphs I and II of compound 1. Rings are defined according to the atom labeling in Figure 3: A: N1–C4, B: N3–C8, C: N5–C12, D: C14–C19.

Rings	Polymorph I	Polymorph II
A–B	87.96 (5)	73.20 (7)
A–C	22.66 (10)	57.19 (11)
B–C	83.37 (4)	79.06 (10)
A–D	78.16 (5)	56.80 (10)
B–D	80.60 (5)	81.78 (10)
C–D	79.78 (5)	79.77 (10)

Table 2. Selected intermolecular interactions in polymorphs of the title compounds.

Polymorph	D–H (Å)	H...A (Å)	D...A (Å)	D–H...A (°)
I				
N7–H7N2...N6 ^a	0.92 (2)	2.33 (2)	3.2463 (19)	178.2 (18)
C10–H10...N4 ^b	0.95	2.65	3.5450 (19)	157.0
II				
N7–H7N2...N6 ^c	0.94 (3)	2.33 (3)	3.199 (3)	152 (2)

Symmetry codes: ^a $-x + 2, -y + 1, -z + 1$; ^b $x + 1, y, z$; ^c $x + 1/2, y - 1/2, z$.

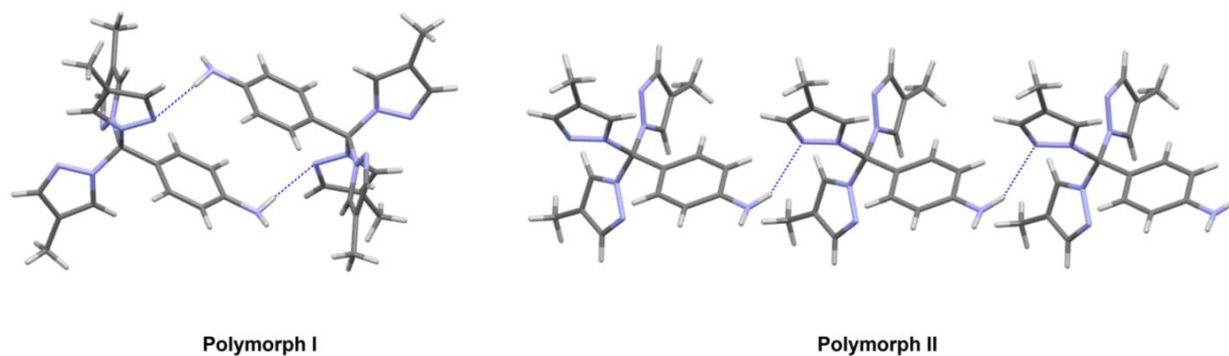


Figure 4. Selected intermolecular interactions (N–H...N as dashed blue lines) in polymorphs I and II of compound 1.

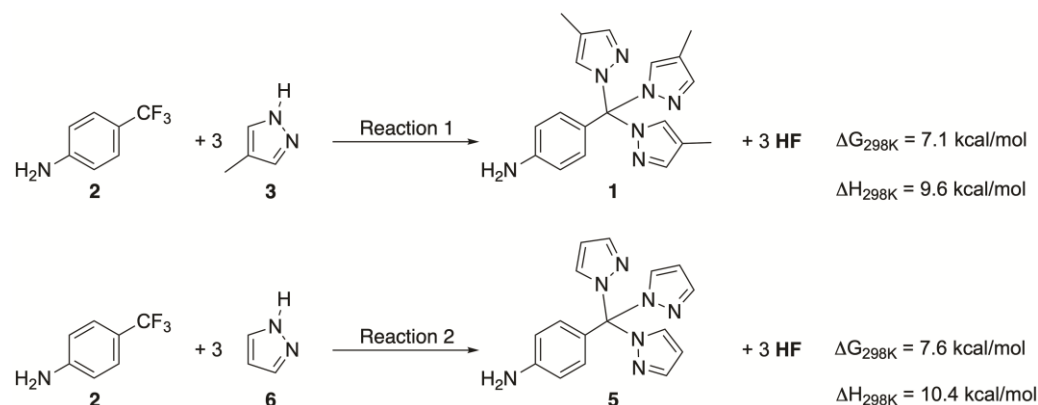


Figure 5. Comparison of energies of two C–F activation reactions.

2.4. Computational Studies

DFT calculations using the MN15-L functional and the def2-TZVP basis set were performed to compare the reaction thermodynamics of the methylpyrazole (3) and the parent unsubstituted pyrazole with 4-(trifluoromethyl)aniline (2) (Figure 5). Optimization and frequency calculations were performed on 4-(tris(4-methyl-1H-pyrazol-1-yl)methyl)aniline (1), 4-(trifluoromethyl)aniline (2), 4-methylpyrazole (3), 4-(tri(1H-pyrazol-1-yl)methyl)aniline (5), pyrazole (6), and hydrogen fluoride. The Gibbs free energy of the reaction to produce 1 (Figure 5, Reaction 1) is calculated to be 7.1 kcal/mol, compared to the Gibbs free energy of the reaction to produce 5 (Figure 5, Reaction 2), which is 7.6 kcal/mol. For the calculated enthalpies of reaction, Reaction 1 has an enthalpy of 9.6 kcal/mol, whereas Reaction 2 has an enthalpy of 10.4 kcal/mol. The calculated Gibbs free energy and enthalpy values indicate that Reaction 1 is more favorable compared to Reaction 2. This small increase in favorability for the methylated compound is attributable to the incorporation of a methyl group into the pyrazole reactant, making it a better nucleophile.

Using the same level of theory, transition states were calculated (Figure 6) for the reactions between 4-(trifluoromethyl)aniline (2) and the two pyrazole derivatives (3 and 6). For this calculation, SMD solvation was included to model the DMSO solvent [15]. Based on pKas and the fact that KOH is present in the reaction conditions, the deprotonated forms of the pyrazole derivatives were selected as the nucleophiles in the transition state calculations [16,17]. As suggested by the computational results, a possible mechanism for product formation involves an S_N2 -type transition state where the deprotonated pyrazole species replaces a fluoride leaving group. The activation energy is slightly lower when deprotonated 4-methylpyrazole (3) is used as a nucleophile, which is again reflective of this species being a better nucleophile. The high activation barriers are consistent with the need for refluxing DMSO (bp = 189 °C).

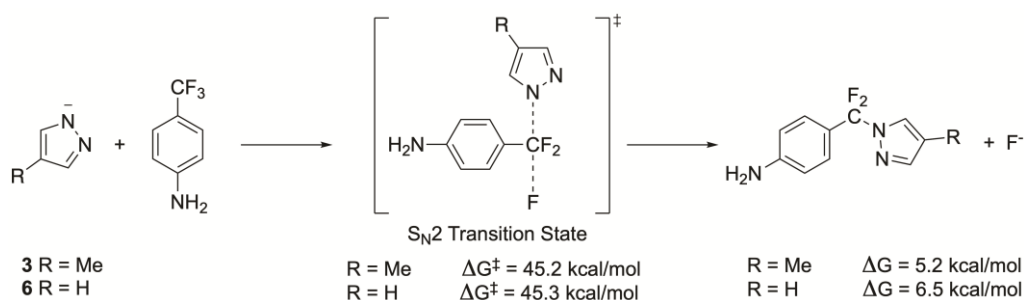


Figure 6. Transition state calculation involved in compound formation.

3. Materials and Methods

All reagents were purchased from commercial suppliers and used as received: 4-(trifluoromethyl)aniline and 4-methylpyrazole (Ambeed, Inc., Arlington Heights, IL,

USA); KOH and DMSO (Fisher Scientific, Hampton, NH, USA). NMR spectra were obtained with a JEOL (Peabody, MA, USA) 400 MHz YH. ^1H NMR resonances were referenced against tetramethylsilane using the residual proton signal, and ^{13}C NMR resonances were referenced against the ^{13}C resonance of CDCl_3 (77.16 ppm) [18]. IR spectra were obtained with a Bruker (Ettlingen, Germany) ALPHA-P. IR data analysis was performed with OPUS version 8.5.

The purified sample was dissolved in LC-MS-grade acetonitrile, and MS data were obtained via direct infusion into a Waters (Milford, MA, USA) Xevo TQD operated in scan mode using the first quadrupole. Electrospray ionization in the positive mode was used with a capillary voltage of 2.5 kV, a cone voltage of 25 V, a desolvation temperature of 250 °C, a desolvation flow of 500 L N_2 /h, and a cone flow of 20 L N_2 /h. The mass spectrum was scanned from m/z 100–900 at 3000 amu/sec. Data analysis was performed with MassLynx version 4.2.

The DFT calculations were performed using Gaussian 16 computation software [19] with the MN15L density functional [20] and def2-TZVP basis set [21]. The MN15-L functional was chosen because of its accuracy in modeling organic molecules with good agreement with experimental trends [22], and the def2-TZVP basis set is reasonably accurate while not being as computationally expensive as its larger relatives [23]. For the transition state calculation, SMD solvation was used to model DMSO [15]. Optimization and frequency calculations were performed on 4-(tris(4-methyl-1H-pyrazol-1-yl)methyl)aniline (1), 4-(trifluoromethyl)aniline (2), 4-methylpyrazole (3), 4-(tri(1H-pyrazol-1-yl)methyl)aniline (5), pyrazole (6), and hydrogen fluoride. Each molecule was benchmarked for accuracy by performing a Root Mean Squared Deviation test for $p \leq 0.05$ and an analysis of the Pearson Correlation Coefficient value x such that $0.90 \leq x \leq 1.00$. These tests were performed on the bond lengths between the computed molecular models and the real molecule's data using R Statistics Software version 4.3.3 [24]. The Gibbs free energy and enthalpy values of the molecules were used to determine the favorability of the reaction between the methyl-substituted aniline product (1) and the unsubstituted aniline compound product (5).

Crystallographic data were obtained at 100 K using a Bruker (Madison, WI, USA) D8 Quest diffractometer with an Incoatec (Geesthacht, Germany) microfocus Mo $K\alpha$ ($\lambda = 0.71073 \text{ \AA}$) source and a Photon III CMOS detector. The APEX4 (2022.10-0) software package [25] was used for instrument control and data processing (SAINT integration and SADABS multiscan absorption correction). The structure was solved by intrinsic phasing (SHELXT) [26] and refined using least-squares techniques (SHELXL) [27]. All non-hydrogen atoms were refined anisotropically. Hydrogen atoms attached to carbon atoms were treated using riding models. Hydrogen atoms attached to nitrogen atoms were identified from the difference in electron density map, and their positions were refined without restraints. Renderings of the crystal structure were generated using Mercury (2023.3.1) [28]. Crystallographic data are summarized in the Supporting Information, Table S1. Data may be obtained in CIF form from the Cambridge Crystallographic Data Centre via CCDC 2344377–2344378.

4-(tris(4-methyl-1H-pyrazol-1-yl)methyl)aniline: A mixture of KOH (1.69 g, 30.1 mmol), 4-(trifluoromethyl)aniline (1.62 g, 10.1 mmol), and 4-methylpyrazole (2.47 g, 30.1 mmol) in 10 mL of DMSO was heated to reflux under N_2 . The yellow heterogeneous mixture changed to a red homogeneous solution before finally becoming yellow and homogeneous during the reflux period. After 1 h, the reaction mixture was diluted with CH_2Cl_2 (100 mL) and washed with $5 \times 20 \text{ mL}$ of NaCl (sat, aq.). The organic layer was dried over MgSO_4 , and the solvent was removed in vacuo. The resulting yellow semi-solid was dissolved in minimal CH_2Cl_2 , purified by column chromatography on silica gel (eluent = Et_2O , $R_f = 0.43$), and subsequently washed with Et_2O ($3 \times 20 \text{ mL}$) to afford the desired product as a white solid (2.18 g, 6.29 mmol, 63%). Note: Because the title compound is insoluble in Et_2O , while collecting fractions, the product occasionally precipitates out of solution. If this occurs, CH_2Cl_2 can be used to redissolve the solid. $^1\text{H-NMR}$ (CDCl_3 , 400 MHz), δ (ppm): 7.50 (s, 3H), 7.25 (s, 3H), 6.88 (d, $J = 8.7 \text{ Hz}$, 2H), 6.62 (d, $J = 8.7 \text{ Hz}$, 2H), 3.85 (s, 2H), 2.05 (s, 9H).

^{13}C -NMR (CDCl_3 , 101 MHz), δ (ppm): 148.1, 141.9, 130.6, 130.1, 127.3, 116.5, 114.2, 92.9, 9.1. IR ν_{max} (cm^{-1}): 3448, 3328, and 1626.

4. Conclusions

We describe the synthesis and characterization of 4-(tris(4-methyl-1*H*-pyrazol-1-yl)methyl)aniline (**1**). The synthesis and purification of this species can be performed in under a day because of the short reaction time needed (1 h) to synthesize this Tp derivative, which contrasts with the lengthy heating periods often required for the synthesis of these ligands (*vide supra*). Crystal growth of **1** fortuitously led to the formation of two polymorphs, differing primarily in the rotational orientation of the pyrazolyl substituents and the resulting N-H \cdots N intermolecular interactions. Specifically, the formation of N-H \cdots N dimers versus N-H \cdots N chains distinguishes polymorphs I and II, respectively. Because the addition of methyl groups is often utilized to increase the solubility of species in organic solvents [29,30], future work will investigate the solubility differences between metal compounds of our title compound and 4-(tri(1*H*-pyrazol-1-yl)methyl)aniline (**5**). Moreover, because other 4-substituted pyrazole ligands (e.g., 4-fluoropyrazole) are commercially available, this strategy may be useful for generating Tp derivatives with varying electronic properties. The generation of novel Tp ligands is advantageous because of their use in catalysis and medicinal chemistry [1–4], and Tp ligands have received less attention compared to their Tpm analogs [3,31].

Supplementary Materials: The following supporting information can be downloaded: Figure S1: ^1H -NMR of title compound in CDCl_3 ; Figure S2: ^{13}C -NMR of title compound in CDCl_3 ; Figure S3: HSQC of title compound in CDCl_3 ; Figure S4: HMBC of title compound in CDCl_3 and NMR assignments based on 2D data; Figure S5: IR of title compound; Figure S6: MS of title compound; Figure S7: Packing diagram of polymorph I, viewed along the *a*-axis; Figure S8: Packing diagram of polymorph II, viewed along the *b*-axis; Figure S9: N-H \cdots N dimers connected into chains via C-H \cdots N interactions in polymorph I. Chains propagate along the *a*-axis; Table S1: Crystallographic data for polymorphs of the title compound.

Author Contributions: Conceptualization, J.A.P.; methodology, B.B.G., J.E.D., N.A., S.J.K.S., K.A.G. and C.D.M.; software, J.E.D., K.A.G. and C.D.M.; validation, B.B.G., J.E.D., N.A., S.J.K.S., J.A.P. and C.D.M.; formal analysis, B.B.G., J.E.D., N.A., S.J.K.S., K.A.G., J.A.P. and C.D.M.; investigation, B.B.G., J.E.D., N.A., S.J.K.S., K.A.G., J.A.P. and C.D.M.; resources, C.D.M., J.A.P., S.J.K.S. and K.A.G.; data curation, B.B.G., J.E.D., S.J.K.S., K.A.G., J.A.P. and C.D.M.; writing—original draft preparation, J.A.P. and C.D.M.; writing—review and editing, B.B.G., J.E.D., N.A., S.J.K.S., K.A.G., J.A.P. and C.D.M.; visualization, B.B.G., J.E.D., S.J.K.S., K.A.G., J.A.P. and C.D.M.; supervision, J.A.P. and C.D.M.; project administration, J.A.P. All authors have read and agreed to the published version of the manuscript.

Funding: This research received no external funding.

Data Availability Statement: CCDC 2344377-2344378 contain the supplementary crystallographic data for this paper. These data can be obtained from the CCDC, 12 Union Road, Cambridge CB2 1EZ, UK; Fax: +44 1223 336033.

Acknowledgments: The authors would like to thank Keenan E. Dungey for his helpful discussions and advice regarding the writing and lab work, John P. Lee for his guidance, both Barbara C. Higgs and Alyssa M. Matthews for double-checking the NMR assignments, and Sarah L. McDarmont for her guidance with the writing.

Conflicts of Interest: The authors declare no conflicts of interest.

References

1. Martins, L.M.D.R.S. C-scorpionate complexes: Ever young catalytic tools. *Coord. Chem. Rev.* **2019**, *396*, 89–102. [[CrossRef](#)]
2. Martins, L.M.D.R.S.; Pombeiro, A.J.L. Water-Soluble C-Scorpionate Complexes—Catalytic and Biological Applications. *Eur. J. Inorg. Chem.* **2016**, *2016*, 2236–2252. [[CrossRef](#)]
3. Muñoz-Molina, J.M.; Belderrain, T.R.; Pérez, P.J. Group 11 tris(pyrazolyl)methane complexes: Structural features and catalytic applications. *Dalton Trans.* **2019**, *48*, 10772–10781. [[CrossRef](#)] [[PubMed](#)]

4. Niesel, J.; Pinto, A.; N'Dongo, H.W.P.; Merz, K.; Ott, I.; Gust, R.; Schatzschneider, U. Photoinduced CO release, cellular uptake and cytotoxicity of a tris(pyrazolyl)methane (tpm) manganese tricarbonyl complex. *Chem. Commun.* **2008**, 1798–1800. [CrossRef]
5. Trofimenko, S. Boron-Pyrazole Chemistry. *J. Am. Chem. Soc.* **1966**, *88*, 1842–1844. [CrossRef]
6. Caballero, A.; Díaz-Requejo, M.M.; Fructos, M.R.; Urbano, J.; Pérez, P.J. Modern Applications of Trispyrazolylborate Ligands in Coinage Metal Catalysis. In *Ligand Design in Metal Chemistry*; Wiley: Hoboken, NJ, USA, 2016; pp. 308–329.
7. Theopold, K.H.; Reinaud, O.M.; Doren, D.; Konecny, R. Dioxygen activation with sterically hindered tris(pyrazolyl)borate cobalt complexes. In *Studies in Surface Science and Catalysis*; Grasselli, R.K., Oyama, S.T., Gaffney, A.M., Lyons, J.E., Eds.; Elsevier: Amsterdam, The Netherlands, 1997; Volume 110, pp. 1081–1088.
8. Slugovc, C.; Padilla-Martínez, I.; Sirol, S.; Carmona, E. Rhodium- and iridium-trispyrazolylborate complexes: C-H activation and coordination chemistry. *Coord. Chem. Rev.* **2001**, *213*, 129–157. [CrossRef]
9. Bromberg, S.E.; Yang, H.; Asplund, M.C.; Lian, T.; McNamara, B.K.; Kotz, K.T.; Yeston, J.S.; Wilkens, M.; Frei, H.; Bergman, R.G.; et al. The Mechanism of a C-H Bond Activation Reaction in Room-Temperature Alkane Solution. *Science* **1997**, *278*, 260–263. [CrossRef]
10. Trofimenko, S. Geminal poly(1-pyrazolyl)alkanes and their coordination chemistry. *J. Am. Chem. Soc.* **1970**, *92*, 5118–5126. [CrossRef]
11. Juliá, S.; del Mazo, J.M.; Avila, L.; Elguero, J. Improved Synthesis of Polyazolylmethanes Under Solid-Liquid Phase-Transfer Catalysis. *Org. Prep. Proced. Int.* **1984**, *16*, 299–307. [CrossRef]
12. Schorpp, M.; Heizmann, T.; Schmucker, M.; Rein, S.; Weber, S.; Krossing, I. Synthesis and Application of a Perfluorinated Ammoniumyl Radical Cation as a Very Strong Deelectronator. *Angew. Chem. Int. Ed.* **2020**, *59*, 9453–9459. [CrossRef]
13. Liddle, B.J.; Gardinier, J.R. A Practical Synthesis of Tris(pyrazolyl)methylaryls. *J. Org. Chem.* **2007**, *72*, 9794–9797. [CrossRef] [PubMed]
14. McDarmont, S.L.; McMillen, C.D.; Temelso, B.; Pienkos, J.A. Exploiting a C–F Activation Strategy to Generate Novel Tris(pyrazolyl)methane Ligands. *Z. Für Anorg. Und Allg. Chem.* **2020**, *646*, 1886–1891. [CrossRef]
15. Marenich, A.V.; Cramer, C.J.; Truhlar, D.G. Universal Solvation Model Based on Solute Electron Density and on a Continuum Model of the Solvent Defined by the Bulk Dielectric Constant and Atomic Surface Tensions. *J. Phys. Chem. B* **2009**, *113*, 6378–6396. [CrossRef] [PubMed]
16. Bordwell, F.G.; Algrim, D.J. Acidities of anilines in dimethyl sulfoxide solution. *J. Am. Chem. Soc.* **1988**, *110*, 2964–2968. [CrossRef]
17. Bordwell, F.G. Equilibrium acidities in dimethyl sulfoxide solution. *Acc. Chem. Res.* **1988**, *21*, 456–463. [CrossRef]
18. Gottlieb, H.E.; Kotlyar, V.; Nudelman, A. NMR Chemical Shifts of Common Laboratory Solvents as Trace Impurities. *J. Org. Chem.* **1997**, *62*, 7512–7515. [CrossRef]
19. Frisch, M.J.; Trucks, G.W.; Schlegel, H.B.; Scuseria, G.E.; Robb, M.A.; Cheeseman, J.R.; Scalmani, G.; Barone, V.; Petersson, G.A.; Nakatsuji, H.; et al. *Gaussian 16 Rev. C.01*; Gaussian, Inc.: Wallingford, CT, USA, 2016.
20. Yu, H.S.; He, X.; Li, S.L.; Truhlar, D.G. MN15: A Kohn–Sham global-hybrid exchange–correlation density functional with broad accuracy for multi-reference and single-reference systems and noncovalent interactions. *Chem. Sci.* **2016**, *7*, 5032–5051. [CrossRef] [PubMed]
21. Daga, L.E.; Civalleri, B.; Maschio, L. Gaussian Basis Sets for Crystalline Solids: All-Purpose Basis Set Libraries vs System-Specific Optimizations. *J. Chem. Theory Comput.* **2020**, *16*, 2192–2201. [CrossRef]
22. Yu, H.S.; He, X.; Truhlar, D.G. MN15-L: A New Local Exchange–Correlation Functional for Kohn–Sham Density Functional Theory with Broad Accuracy for Atoms, Molecules, and Solids. *J. Chem. Theory Comput.* **2016**, *12*, 1280–1293. [CrossRef]
23. Weigend, F.; Ahlrichs, R. Balanced basis sets of split valence, triple zeta valence and quadruple zeta valence quality for H to Rn: Design and assessment of accuracy. *Phys. Chem. Chem. Phys.* **2005**, *7*, 3297–3305. [CrossRef]
24. R Core Team. *R: A Language and Environment for Statistical Computing*; R Foundation for Statistical Computing: Vienna, Austria, 2017. Available online: <https://www.R-project.org/> (accessed on 27 March 2024).
25. Bruker. *APEX4*; Bruker AXS Inc.: Madison, WI, USA, 2017.
26. Sheldrick, G. SHELXT—Integrated space-group and crystal-structure determination. *Acta Crystallogr. Sect. A* **2015**, *71*, 3–8. [CrossRef]
27. Sheldrick, G. Crystal structure refinement with SHELXL. *Acta Crystallogr. Sect. C* **2015**, *71*, 3–8. [CrossRef] [PubMed]
28. Macrae, C.F.; Sovago, I.; Cottrell, S.J.; Galek, P.T.A.; McCabe, P.; Pidcock, E.; Platings, M.; Shields, G.P.; Stevens, J.S.; Towler, M.; et al. Mercury 4.0: From visualization to analysis, design and prediction. *J. Appl. Crystallogr.* **2020**, *53*, 226–235. [CrossRef] [PubMed]
29. Paton, A.S.; Lough, A.J.; Bender, T.P. One Well-Placed Methyl Group Increases the Solubility of Phenoxy Boronsubphthalocyanine Two Orders of Magnitude. *Ind. Eng. Chem. Res.* **2012**, *51*, 6290–6296. [CrossRef]
30. Pinheiro, P.S.M.; Franco, L.S.; Fraga, C.A.M. The Magic Methyl and Its Tricks in Drug Discovery and Development. *Pharmaceuticals* **2023**, *16*, 1157. [CrossRef]
31. Reger, D.L. Tris(Pyrazolyl)Methane Ligands: The Neutral Analogs of Tris(Pyrazolyl)Borate Ligands. *Comments Inorg. Chem.* **1999**, *21*, 1–28. [CrossRef]

Disclaimer/Publisher’s Note: The statements, opinions and data contained in all publications are solely those of the individual author(s) and contributor(s) and not of MDPI and/or the editor(s). MDPI and/or the editor(s) disclaim responsibility for any injury to people or property resulting from any ideas, methods, instructions or products referred to in the content.